ELSEVIER

Brain Research 934 (2002) 87–96

BRAIN RESEARCH

www.elsevier.com/locate/bres

Research report

Volumetric structural magnetic resonance imaging (MRI) of the rat hippocampus following kainic acid (KA) treatment

O.T. Wolf[c,e,f], V. Dyakin[a], A. Patel[e], C. Vadasz[a,d], M.J. de Leon,[b,c], B.S. McEwen[e], K. Bulloch[e,*]

[a]*Laboratory of Neurobehavioral Genetics, Nathan S. Kline Institute for Psychiatric Research, Orangeburg, NY 10962, USA*
[b]*Nathan S. Kline Institute for Psychiatric Research, Orangeburg, NY 10962, USA*
[c]*Center for Brain Health, Neuroimaging Lab., NYU School of Medicine New York, New York, NY 10016, USA*
[d]*Department of Psychiatry, NYU School of Medicine, New York, NY 10016, USA*
[e]*Laboratory of Neuroendocrinology, Rockefeller University, P.O. Box 165, 1230 York Ave., New York, NY 10021, USA*
[f]*Institute of Experimental Psychology, University of Duesseldorf, 40225 Duesseldorf, Germany*

Abstract

An in vivo MRI study employing a high field (7T) magnet and a T1- and T2-weighted imaging sequence with subsequent histopathological evaluations was undertaken to develop and evaluate MRI-based volumetric measurements in the rat. The brain structures considered were the hippocampus, the cingulate cortex, the retrosplenial granular cortex and the ventricles. Control ($n=3$) and kainic acid (KA; $n=4$) treated rats were scanned 10 days following the manifestation of stage four seizures. The MRI images exhibited anatomical details (125 μm in-plane resolution) that enabled volumetric analysis with high intra-rater reliability. Volumetric analysis revealed that KA-treated rats had significantly smaller hippocampi, and a significant increase in ventricular size. The cingulate cortex and the retrosplenial granular cortex did not differ in volume between the two groups. The histological observations supported the MRI data showing neuronal loss and neuronal degeneration in CA1 and CA3 of the hippocampus, which was accompanied by strong microglia activation. These data demonstrate a reliable and valid method for the measurement of the rat hippocampus in vivo using MRI with a high field magnet, thereby providing a useful tool for future studies of rodent models of neuro-degenerative diseases. © 2002 Elsevier Science B.V. All rights reserved.

Theme: Disorders of the nervous system

Topic: Neurotoxicity; Human studies; Animal models

Keywords: Magnetic resonance imaging (MRI); Volumetric measurement; Hippocampus; Kainic acid; Rats; Microglia; Neurodegeneration; Ventricles; In vivo

1. Introduction

Volumetric estimation using structural magnetic resonance imaging (MRI) is widely used in human neuroscience research, in particular, in the study of epilepsy [45], Alzheimer's disease [17], and schizophrenia [11,22]. Traditional anatomical methods used in animal research are typically conducted post mortem, e.g., neuron counting, spine density measurements, dendritic length measurements [25,34,46]. While these methods have the advantage of a detailed analysis with a high resolution, they exclude the possibility to measure the same parameter longitudinally in individual animals. Advances in the design of MRI magnets with high field-strength and in their use for obtaining images of the brain, as well as progress in image analysis software has made the in vivo MRI of smaller animal brains possible.

Indeed in vivo MRI has been used in several experimental rodent models to detect induced structural damage by investigating changes in perfusion coefficients, tissue relaxation parameters, lesion sizes, or ventricular volumes [4,5,9,21,29,31,35,37,43,44]. Moreover some studies reported that their results were in good agreement with histological observations [1,6,27].

Little information exists for volumetric studies of small animal brains using MRI even though early studies have

*Corresponding author. Tel.: +1-212-327-8623; fax: +1-212-327-8634.

E-mail address: bullock@rockvax.rockefeller.edu (K. Bulloch).

0006-8993/02/$ – see front matter © 2002 Elsevier Science B.V. All rights reserved.
PII: S0006-8993(02)02363-6

already identified and described brain structures like the cingulate gyrus or the hippocampus on their acquired images (e.g., Refs. [7,16,18,19,27]). One previous paper describes a protocol to measure the hippocampus in tree shrews [32]. However, to our knowledge no detailed protocols (with demonstrated reliability) for volumetric studies of the rodent hippocampus are available to date. The present study was therefore undertaken with three goals: first, to develop a reliable method to measure the volumes of the hippocampus, the cingulate cortex, the retrosplenial granular cortex, and the ventricles using MRI images; second, to validate these methods using a well-characterized hippocampal lesion model, i.e., kainic acid (KA)-induced seizures, which lead to neuronal degeneration and cell death in the hippocampus [40]; and third, to qualitatively characterize histo-pathological changes in the regions evaluated by MRI.

2. Materials and methods

2.1. Animals

Seven out of a total of sixteen 8-week-old adult male Sprague–Dawley rats (295.8±4.4 g mean±S.E.) were selected for this experiment. At the time of the MRI experiment (10 days later) the weight of the rats was 351±15 g). All animals were housed in accordance with the Animal Welfare Act [30], given free access to food (rat chow) and water, and kept on a 12:12-h light/dark cycle.

2.2. Kainic acid (KA) treatment

The experimental rats received one i.p. injection of KA (16 mg/kg) or placebo (saline). Thereafter, animals were observed for 3 h for behavioral symptoms of seizure activity. Animals achieving stage four seizures according to the classification of Lothman and Collins [23] (e.g., upper and lower body clonus, salivation, wet dog shake) were considered in this study. Once they displayed seizure behavior, the rats received an i.p. injection of Nembutal (ranging from 25 to 36 mg/kg) in order to stop seizure activity. Thereafter, animals were kept in the housing facility for 10 days. Four animals which had received KA and three animals from the control group were selected for this experiment. Animals were transferred to the MRI facility of the Nathan S. Kline Institute for Psychiatric Research (Orangeburg, NY), where the MRI scans were acquired. Thereafter they were transferred back to Rockefeller University (New York, NY) for perfusion and histological analysis.

2.3. MRI system

A 7.0-Tesla 40-cm horizontal bore MR system (Magnex Scientific, Abingdon, UK), driven by a Surrey Medical Imaging Systems (SMIS, Guilford, UK) spectrometer was used. The system is equipped with a rodent imaging gradient set (10 cm I.D. 1000 mT/m, 200 ms rise time). A quadrature bird-cage transmit/receive radio-frequency (RF) coil (Morris Instruments, Canada) was employed.

2.4. MRI sequence

A moderate spin-echo sequence (TR 4000 ms and TE 25 ms, four averages, 0.6-mm slice thickness with a 0.3-mm gap, slice interleave 2; bandwidth −25 KHz, RF pulse with shape of five lobe sinc and BW 3 kHz optimized for reasonable signal-to-nose ratio and contrast in the considered brain structures was employed for acquisition of T1- and T2-weighted images. Other groups have used similar sequences for MRI of the mouse brain and tree shrew brain at 2.4 Tesla [28,32]. The field of view (FOV) was 32×32 mm, the matrix was 256×256 resulting in an in-plane resolution 125 μm. First a sagittal scout image was taken to control for proper image alignment. The acquired coronal sections used for the volumetric analyses were taken perpendicular to a line connecting the superior end of the olfactory bulb with the superior end of the cerebellum. A total of 28 sections were taken and the approximate scan time was 70 min per animal. Total time (shimming, scout image acquisition and actual acquisition) in the magnet was around 120 min.

2.5. Animal preparation for the MRI scanning

Animals were first lightly anesthetized with 3% isoflurane in 75% NO_2+25% O_2, followed by an i.p. injection of 20 mg/kg diazepam (Elkins-Sinn, Cherry Hill, NJ). For maintenance of anesthesia during experiment, isoflurane was reduced to 1.5% with slight correction for body weight. Temperature was monitored throughout the scan using a rectal probe. Body temperature was controlled through a water containing line system, with automatic temperature monitoring. The animal's head was fixed in a head holder (David Kopf Instruments, Tujunga, CA), and limb movements were controlled by wrapping the animal with a flexible textile, which allowed breathing but prevented limb movements.

2.6. Volumetric analyses

The MRI scans were transferred to a Sun computer station, where volumetric analysis was performed using an in house developed image analysis program (MIDAS, Wai Tsui, NYU unpublished).This program allows the user to manually outline regions of interest (ROIs) and afterwards calculate the volumes of a specific ROI. The originally acquired coronal images were used for the volumetric analysis. For all ROIs the measures for both hemispheres were combined.

The hippocampus (cornu ammonis, CA) and dentate

gyrus (DG) was manually outlined on coronal slices from rostral to caudal. The starting rostral slice was defined by the CA and DG and coincided with the dorsal hippocampal commissure approximately −2.12 mm from bregma [33]. Multiple features defined the caudal boundary: the loss of contrast between the external capsule and the subiculum, the absent DG and the clear separation of the two cerebral hemispheres. This level corresponds to ca. −6.8 mm from bregma. In all animals the hippocampus was measured on six consecutive slices. In addition the hippocampus was divided into its dorsal and ventral portion. The dorsal part ranged from ca. −2.12 to −3.8 mm from bregma, which corresponded to three slices on the MRI, while the ventral part ranged from ca. −4.5 to ca. −6.8 mm from bregma, which again corresponded to three slices on the MRI. See Fig. 1 for examples of ROIs for the dorsal and ventral hippocampus.

The cingulate cortex (areas 1 and 2; [33]) was outlined by starting at the intersection of corpus callosum with the midline and following the corpus callosum and cingulum to its most dorsolateral point. This point was then connected to the most dorsal and medial intra-hemispheric point of the cortex. Using this landmark based method the cingulate cortex was measured on four slices starting rostrally at the closure of the genu of the corpus callosum (ca. 1.6 mm from bregma) and terminating caudally at the rostral limit of the hippocampus (ca. −1.4 mm from bregma). While providing a standardized method for volume estimation this measure excludes rostrally a certain amount of cingulate (area 1; see Ref. [26]). See Fig. 1 for an example of the cingulate cortex ROI.

The retrosplenial granular cortex (rsg; area b) is the caudal continuation of the cingulate and was measured in a similar fashion as the cingulate gyrus. The retrosplenial granular cortex was measured on four consecutive slices starting rostrally at the rostral limit of the hippocampus (approximately −2.12 mm from bregma, see above). The caudal termination was defined as the slice prior to the opening of the corpus callosum, which is approximately −5.3 mm from bregma [33]. See Fig. 1 for an example of the retrosplenial granular cortex ROI.

2.6.1. Ventricular CSF volume

Using a threshold function with additional manual editing, the ventricular CSF volume (lateral ventricle, third ventricle, and aqueduct) was determined for each slice, which was used for volumetric analysis (10 slices). In the KA-treated animals this measurement might also contain a certain amount of damaged tissue with severe gliosis, which could result in a signal hyperintensity difficult to distinguish from the CSF with the current MRI protocol.

2.6.2. Intracranial vault

In order to control for possible differences in global brain volume, the entire brain was outlined on the 10 slices, which were used for cingulate or hippocampal measurements.

2.7. Histochemistry and immunocytochemistry

2.7.1. Perfusion protocol

Rats were lethally anesthetized with Nembutal, perfused transcardially, sequentially with (A) 10 ml of heparinized normal saline, (B) 60 ml of 3.75% acrolein in 2% paraformaldehyde in 0.1 M phosphate buffer (PB) pH 7.6, and (C) 200 ml of 2% paraformaldehyde in PB. Five-mm thick coronal blocks of the forebrain containing the hippocampal formation were removed and post-fixed in 2% paraformaldehyde in PB for an additional 30 min. Sections (40 μm) were cut on a vibrating microtome and collected into PB. Hippocampal sections were chosen from the dorsal region corresponding to bregma −3.3 mm and from the ventral region corresponding to bregma −5.30 mm [33]. The plane of section was selected to match as closely as possible the plane of section in the MRI imaging. Matched sections from saline- and KA-treated rats were processed simultaneously and stained with Cresyl Violet, Fluoro-Jade, OX-42 and GFAP (see below).

2.7.2. Cresyl Violet staining

A standard protocol from Carleton's histological technique [14] was used to stain the sections with Cresyl Violet (CV).

2.7.3. Fluoro-Jade labeling

Degenerating neurons were visualized using the procedure by Schmued et al. [38].

2.8. Antibody labeling protocol

2.8.1. Microglial and astrocyte markers

A longer description of the used protocol is given in a previous publication [13]. For identification of microglia, a monoclonal antibody OX-42 (Serotec, NC) was used that is specific for the C3b1 receptor, otherwise known as CD11b [36]. A monoclonal antibody (Boehringer-Mannheim, Indianapolis, IN) against glial fibrillary acidic protein (GFAP) was used to identify astrocytes (see Ref. [13]). All antibodies were tested for specificity by preabsorption with the specific protein or peptide.

2.9. Light and fluorescence microscopy

A Nikon fluorescence and light photomicroscope was used to evaluate and photograph the control and KA-treated rat brains. Changes in Fluoro-Jade labeling as well as OX 42-immunoreactivity (IR) and GFAP-IR were qualitatively recorded at the level of the dorsal and ventral hippocampus.

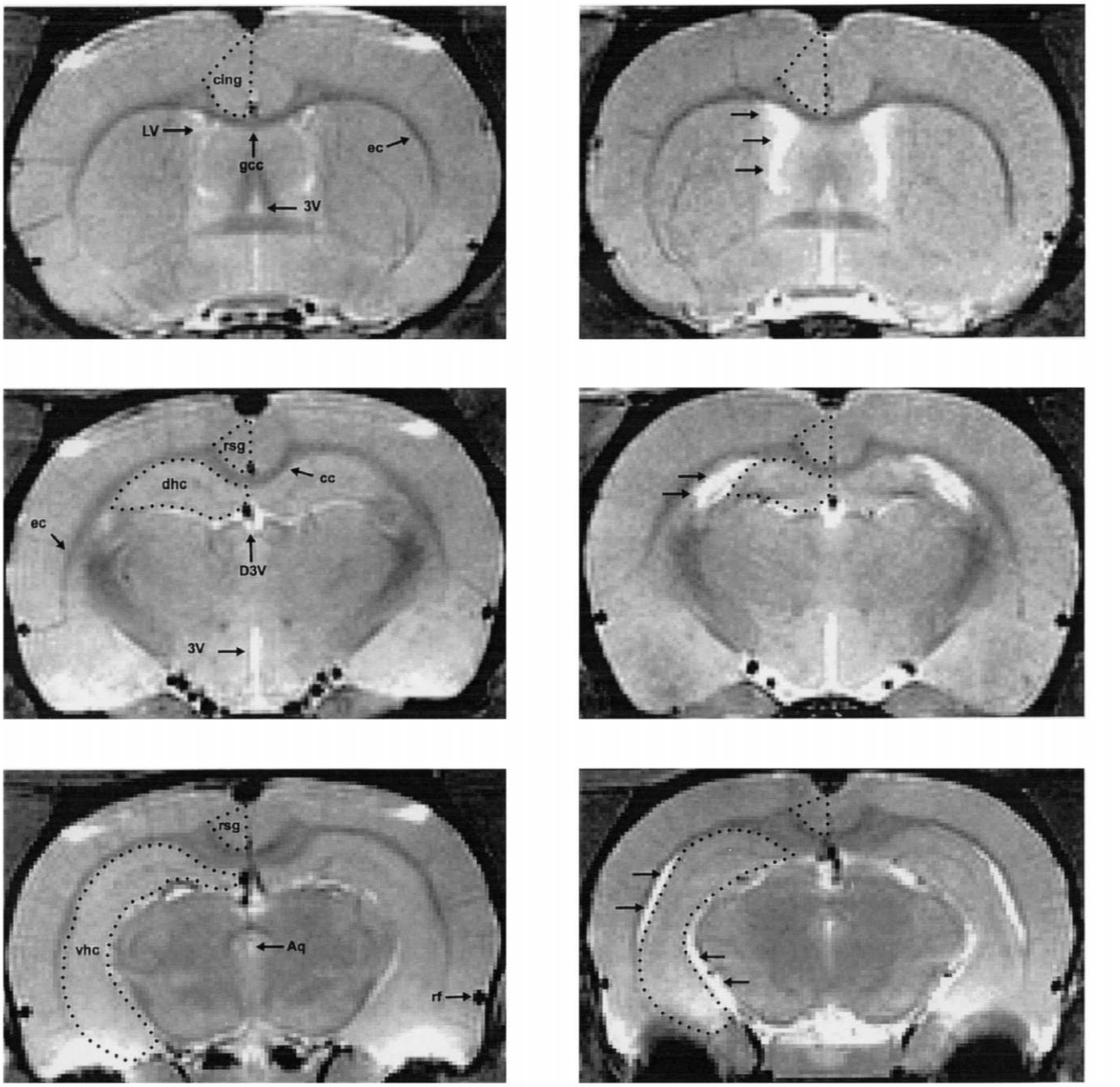

Fig. 1. MRI scans of a control (left side) and a KA-treated animal (right side) at the level of the cingulate cortex (approximately −0.30 mm from bregma) (upper row); the dorsal hippocampus (approximately −3.3 mm from bregma) (middle row); the ventral hippocampus (approximately −5.3 mm from bregma) (lower row). Examples of the ROI drawings for the cingulate cortex (cing), the retrosplenial granular cortex (rsg), the dorsal hippocampus (dhc), and the ventral hippocampus (vhc) used for the volumetric analysis are shown on the left side of each slice. For ease of presentation the drawings are shown as dots in order to allow a view of the underlying anatomy. For the actual analysis these dots are joined in order to create an outline of the region. The black arrows on the slices from the KA-treated animal show the lesion induced signal hyperintensities, which reflect an increased water signal. Some additional anatomical landmarks are indicated on the scan from the control animal (cc, corpus callosum; gcc, genu of the corpus callosum; ec, external capsule; LV, lateral ventricle; D3V, dorsal third ventricle; Aq, aqueduct; rf, rhinal fissure).

2.10. Statistics for MRI

2.10.1. MRI volumetric reliability

The same rater (OTW) outlined the ROIs of the three control and four KA-treated animals again after a period of 7 days in order to assess intra-rater reliability. Reliability was measured at the level of the total volume ($n=7$) and at the level of the slice ($n=21–70$ depending on the number of slices measured for the specific region) using intraclass correlation coefficient (r_{icc}) [39].

2.10.2. MRI volumes

Because of the small sample sizes the nonparametric Mann–Whitney *U*-test was used to compare the two treatment groups.

3. Results

3.1. MRI-derived volumes

High intra-rater reliability was observed for the MRI-derived volumetric assessment of the regions. This was the case for the total volume ($r>0.95$) and for the determination at the slice level ($r>0.93$). Lowest reliability was achieved for the ventricles. Highest reliability was achieved for the hippocampus and the intracranial vault ($r=0.99$).

The experimental and control group did not differ in intracranial vault (Controls: 1064.7 ± 17.3 mm^3; KA: 1064.7 ± 17.1 mm^3; $Z=0$, $P>0.10$). However, KA-treated animals had a significantly reduced hippocampal volume ($Z=2.12$, $P<0.05$) and an increased ventricular volume ($Z=2.12$, $P<0.05$) (Fig. 2). If the two parts of the hippocampus were analyzed separately, the dorsal hippocampus showed a trend in volume reduction by KA ($Z=1.4$, $P=0.15$), where as the ventral hippocampus was significantly smaller in the KA-treated animals ($Z=2.12$, $P<0.05$). The cingulate ($Z=-0.53$, $P>0.10$) and retrosplenial granular cortex ($Z=-0.53$, $P>0.10$) volumes were not different between the two groups (Fig. 2).

3.2. Histological data

3.2.1. Cresyl Violet

Compared to control rats slices from KA-treated rats showed a decreased neuronal density (large labeled cells) in hilus of the DG, CA1 and CA3, but an increase in smaller labeled cells (reflecting glia cells). No changes from control rats were observed in the cingulate and retrosplenial granular cortex (data not shown).

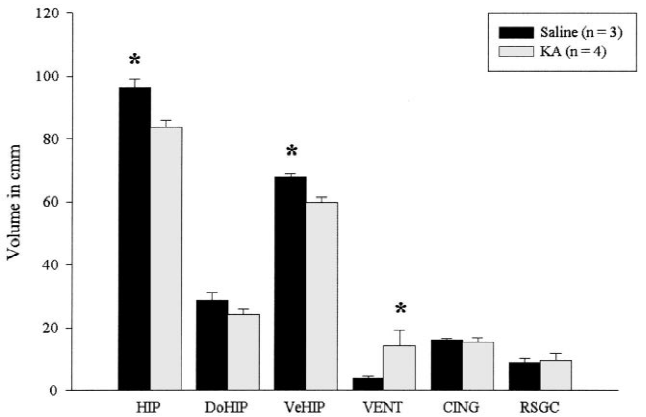

Fig. 2. MRI-derived volumes for hippocampus (HIP), dorsal hippocampus (DoHIP), ventral hippocampus (VeHIP), ventricles (VENT), cingulate cortex (CING), retrosplenial granular cortex (RSGC). *$P<0.05$.

3.2.2. Fluoro-Jade

No stained neurons were observed in any brain region in control rats (Fig. 3A). Strong Fluoro-Jade staining (indicating degenerating neurons) was observed in the pyramidal cell layers in CA3 and CA1 as well in the hilus of the dentate. The ventral hippocampus was more affected, especially CA1 (Fig. 3B–G). No evidence for degenerating neurons was detected in the cingulate cortex and retrosplenial granular cortex (data not shown).

3.2.3. Microglia activation

Within the hippocampus of the control group OX-42 immunoreactivity was observed in microglia cell bodies and in their thin processes. These small stained cells were uniformly distributed throughout the hippocampus within the stratum radiatum (SR), stratum oriens (SO), and the hilus. Rare microglia cell bodies and a few processes were seen in CA1, CA2, CA3 and the granule cell layer (GCL). See Figs. 4 and 5. In KA-treated animals activated and non-activated microglia cells were observed. Activated microglia have larger cell bodies with thicker processes. Within the hippocampus, the largest amount of activated microglia was evident in SR, SO and pyramidal cell layers of CA1 followed by CA3. A less pronounced immunoreactivity of activated microglia was present in the hilus. In addition to the hippocampus, strong microglia activation was seen in the rostral entorhinal area, with less evident activation in the more caudal regions (see Fig. 5). The distribution of non-activated microglia was similar to controls in the cingulate cortex and retrosplenial granular cortex (see Fig. 5).

3.2.4. Astroglia activation

GFAP immunoreactivity was observed in small cells with very thin radial processes throughout the dorsal or ventral hippocampus. Staining was evenly distributed within the SO, SR, the polymorphic layer of the DG, and the pyramidal cell layer of CA1 and CA3. While labeling revealed most of the cells to be small with thin processes, some cells displayed very long processes extending through the DG. Overall, there were no obvious regional differences. In KA-treated rats, there were no apparent differences in the GFAP-immunoreactivity staining pattern compared to controls, indicating that no astroglia activation was apparent 10 days after KA treatment (data not shown).

4. Discussion

4.1. Assessment of hippocampal volumes

The present study describes a volumetric method for the

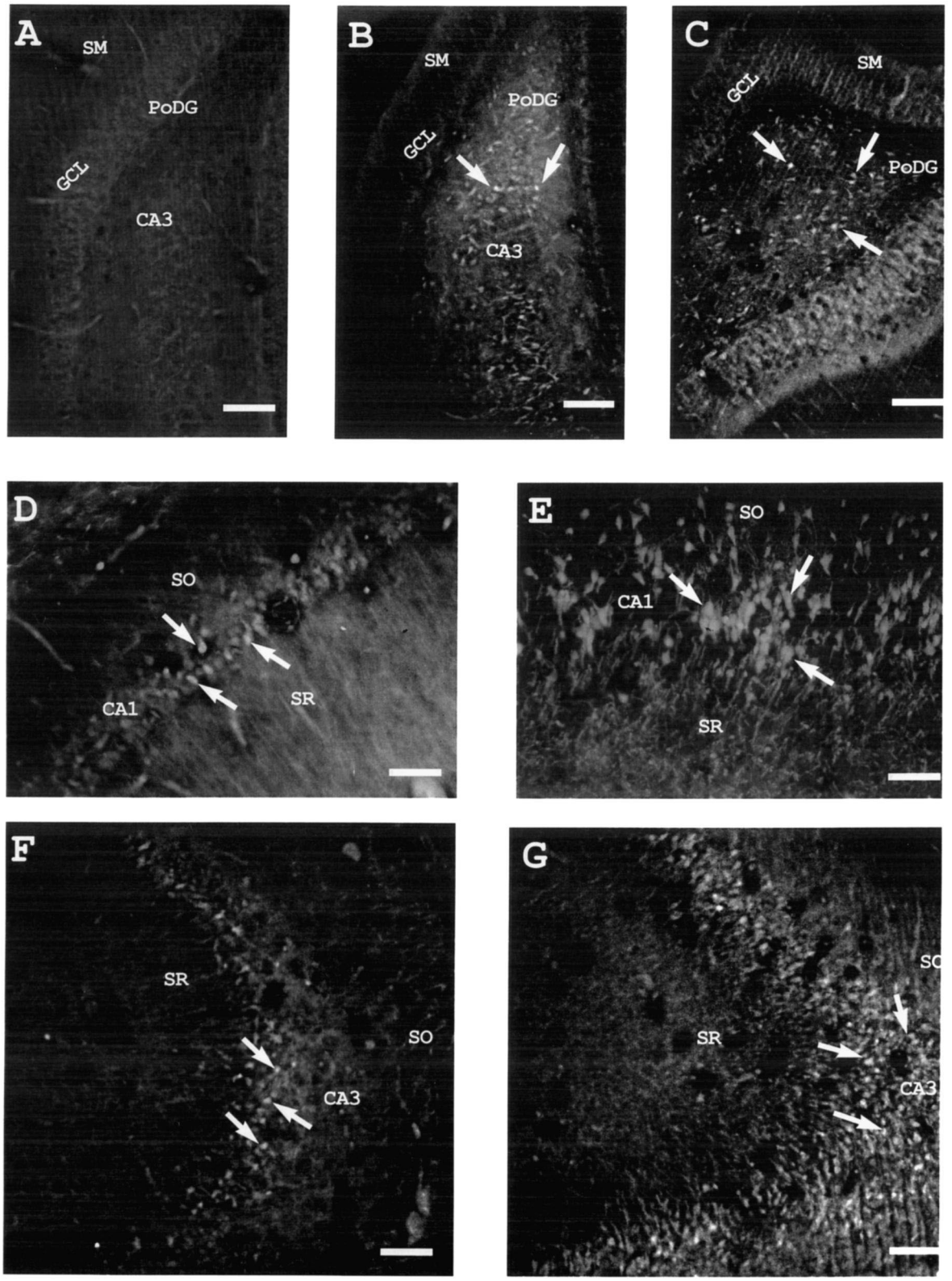

Fig. 3. Fluoro-Jade-labeled sections showing (A) sections from a control animal and (B–G) sections from a KA-treated animal. (A) A dorsal DG section of a control animal (magnification, ×10). Note the complete absence of any signal (the brightly stained degenerating neurons visible in the KA-treated animals). (B) Dorsal DG (magnification, ×10); (C) ventral DG (magnification, ×10); (D); dorsal CA1 (magnification, ×20); (E) ventral CA1 (magnification, ×20); (F) dorsal CA3 (magnification, ×10); (G) ventral CA3 (magnification, ×10). The white arrows point to examples of stained degenerating neurons in the hilus of the dentate gyrus (B,C) and in the pyramidal cell layers of CA1 (D,E) and CA3 (F,G). Note that for all three regions of the hippocampus there are more degenerating neurons in the ventral parts, when compared to the dorsal parts. The measurement bar equals 200 μm for the ×10 magnified sections and 100 μm for the ×20 magnified sections (D,E). Abbreviations: IML, inner molecular layer; PoDG, polymorph layer of the dentate gyrus; GCL, granular cell layer; SO, stratum oriens; SR, stratum radiatum.

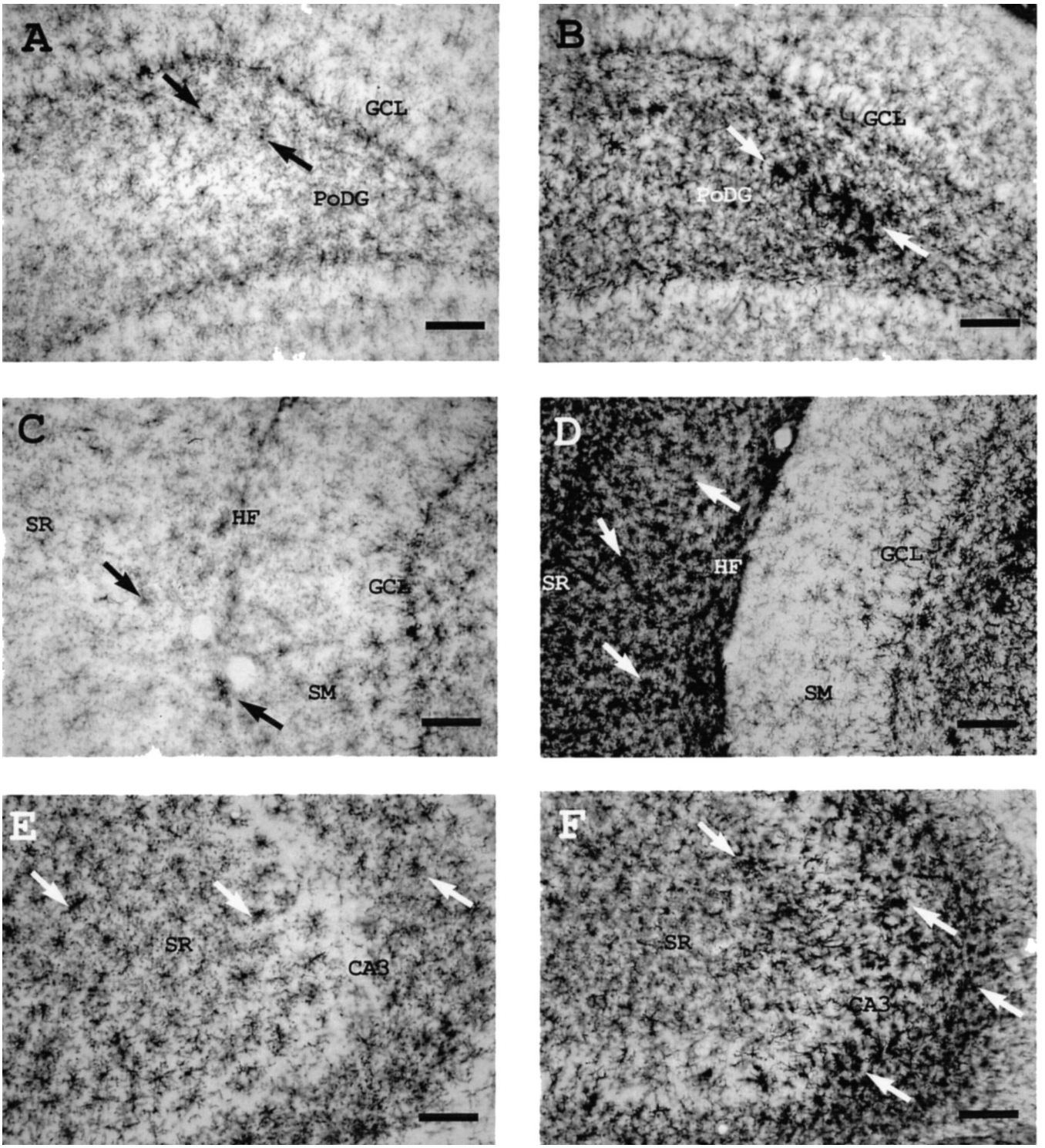

Fig. 4. Dorsal section showing OX 42 staining (magnification, ×10) in a control (left side) and a KA-treated animal (right side). (A,B) Dorsal DG; (C,D) dorsal CA1; (E,F) dorsal CA3. The arrows point to activated microglia, which are rarely seen in the control sections, but occur in high densities in KA-treated animal. The measurement bar equals 100 μm. Abbreviations: PoDG, polymorph layer of the dentate gyrus; GCL, granular cell layer; SO, stratum oriens, stratum radiatum; SM, stratum molecularis; HF, hippocampal fissure.

measurement of the rat hippocampus and also establishes methods for the assessment of cortical brain structures (cingulate cortex and retrosplenial granular cortex) and total ventricular volume. We imaged the rat brain with a high field strength (7T) magnet and a T1- and T2-weighted sequence, which results in a scan with sufficient anatomical contrast to determine regional brain volumes. In the current study the cortical regions were used as control

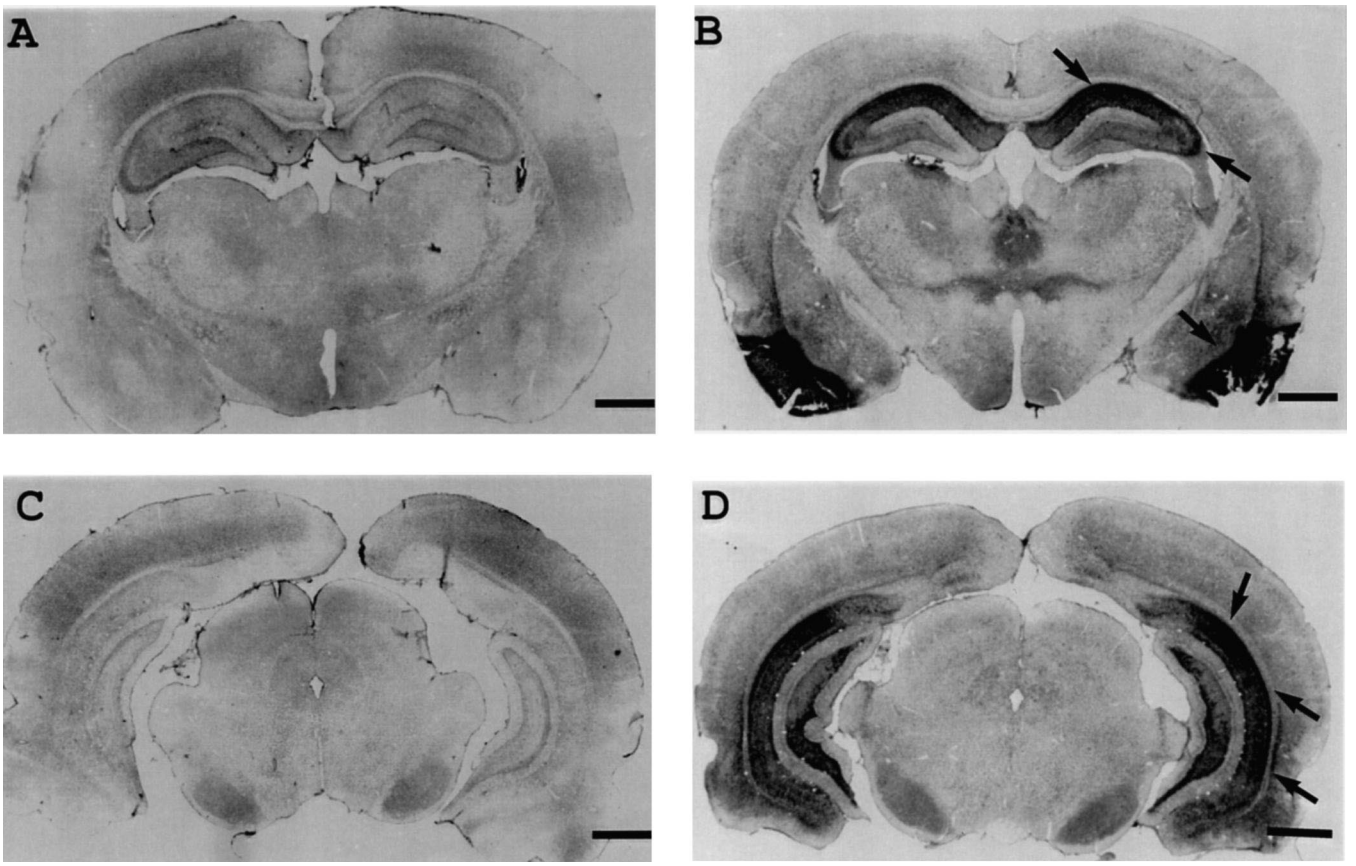

Fig. 5. Scanned slice of OX-42 stained sections at the level of the dorsal (upper row) and ventral (lower row) HC of a control (left side) and a KA (right side) treated rat. Note the strong microglia activation in the dorsal and ventral HC and the complete absence of a similar activation in the neocortical regions. The measurement bar equals 1.2 mm.

regions in order to evaluate the anatomical specificity of the KA damage. In the past a similar approach was employed (using the superior temporal gyrus as a control region) in several human studies investigating the anatomical correlates of cognitive decline during human aging (e.g., Refs. [15,24]).

The measurement of the intracranial vault allowed us to ascertain that the observed differences in hippocampal volume are not caused by baseline differences in brain size and/or global effects on brain volume. If differences in total intracranial vault are observed between experimental groups, the intracranial vault should be used as a covariate or as the denominator in a ratio [26].

4.2. Interpretation of MRI images of kainate-damaged hippocampus

In vivo MRI in rats treated with KA has been used previously to assess changes in diffusion coefficients and T2 relaxation parameters [9,21,29,35,44]. However, to the best of our knowledge there is no previous study which used a volumetric approach in combination with several qualitative histological markers of neuronal degeneration, neuronal loss, and glial reactivity.

The MRI of KA-treated rats showed enlarged ventricles. However, our T1- and T2-weighted sequence might produce hyperintensity signal in adjacent areas of severe gliosis and/or edema (see discussion below) thus partially confounding the measurements of ventricular CSF. Volumetric analysis of the MRI images demonstrate a significant reduction in hippocampal volume of the experimental rats 10 days following KA injection, whereas the cingulate cortex, retrosplenial cortex, and total brain volumes of these animals were not changed. This finding corresponds well with the known neuropathological lesions induced by KA treatment [23] and with our own histological observations.

Fluoro-Jade evaluation of the KA-treated and control rat brains demonstrated substantial neuronal degeneration in the hippocampus. These results indicate that even 10 days after the KA injection neuronal degeneration is still ongoing. Moreover, an already established neuronal loss could be demonstrated using Cresyl Violet stain.

The qualitative analysis of the histology section supported the observed dorsal to ventral gradient of lesion severity, with the ventral part being more affected. This regional pattern was most clearly detectable for Fluoro-Jade labeled degenerating neurons. In line with this, we

found with MRI that only the ventral hippocampus showed a significant volume reduction, while the dorsal hippocampus only tended to be reduced. However, because of the small sample size these results have to be confirmed in a larger study. The observation that the ventral hippocampus is more affected by KA treatment, however, is in agreement with previous histological studies [12,23].

4.3. Glial reactions after KA treatment and ventricular volume change

There was a marked difference between microglia and astrocyte activation in KA treated brain tissue 10 days after the treatment. The microglia marker OX 42 showed many activated microglial cells in the CA1 and CA3 region. In contrast, astroglial activation was almost totally absent. This follows a similar pattern to that produced by trimethyltin lesions [13] and indicates that the astrocyte response to KA-induced damage was not as robust as that of microglia under the conditions and survival time used in the present study. Strong microglia activation with little or no astrocyte activation several days after KA injection has been observed by some groups (e.g., Refs. [2,20] but not others [3]. Since these reactions appear to be time- and dose-dependent, generalization from our data to other time points after KA injection or to other used doses cannot be made.

The pattern of microglial activation within the hippocampus corresponded with the regions of damage indicated by the MRI signal hyperintensities suggesting that these MRI changes in vivo might in part reflect a change in microglia activation. Indeed it is well known that hyperintensities occurring in T2-weighted images can be reflective of gliosis and the accompanying increase in tissue water content (e.g., Refs. [9,10]). However, the areas within the hippocampus where microglia activation was apparent were much larger than the areas of MRI signal hyperintensities. Nevertheless it might be that the signal hyperintensity partially reflects microglia activation and its associated water accumulation. This might explain why the ventricular enlargement seen on MRI seemed to be less apparent in the qualitative histological observations (e.g., when one compares the MRI image (Fig. 1) with the scanned OX 42 section (Fig. 5)).

Another reason for the discrepancy between histological and MRI derived sections could be local edema (swelling), which also results in MRI signal hyperintensities. Indeed edema and gliosis are two processes which often occur simultaneously and/or in a serial pattern after neuronal damage due to seizure or stroke [9,41,42].

Finally the histological procedures of dehydration, fixation and mounting reduces the ventricular volumes as seen post mortem [4,6]. Future studies could use multiple MRI sequences in order to disentangle the contribution of ventricular CSF versus gliotic tissue in creating the hyperintensities observed with the current sequence.

The present study used histological samples in order to qualitatively characterize and illustrate the KA-induced damage. An important future step would be to validate the method in a quantitative fashion using volumes derived from histology in addition to stereologically derived neuronal counts for comparison with the MRI-derived data. This approach has been proven fruitful in our human post mortem validation studies [8] and has been used in several rodent studies for the measurement of ventricular volumes and lesion sizes [1,4,6].

In conclusion, the volumetric method presented here is a first step in providing the tools needed to conduct volumetric research in rodent models of neurodegenerative diseases. Using the KA lesion model in combination with qualitative histological analysis we have given one example for the potential use of this method.

Acknowledgements

Supported by grants from the NIH [MH 41256, MH42834 (BSM, KB)], NIH, NIA [AG 08051, AG 12101(MdL)]; the Dreyfus Health Foundation N.Y and NIH AA11031 (CV), the Deutsche Forschungs Gesellschaft (WO-733/1-1; OTW).

References

[1] P.R. Allegrini, D. Sauer, Application of magnetic resonance imaging to the measurement of neurodegeneration in rat brain: MRI data correlate strongly with histology and enzymatic analysis, Magn. Reson. Imaging 10 (1992) 773–778.
[2] P.B. Andersson, V.H. Perry, S. Gordon, The kinetics and morphological characteristics of the macrophage-microglial response to kainic acid-induced neuronal degeneration, Neuroscience 42 (1991) 201–214.
[3] M. Araujo, F. Wandosell, Differential cellular response after glutamate analog hippocampal damage, J. Neurosci. Res. 44 (1996) 397–409.
[4] Y. Assaf, E. Beit-Yannai, E. Shohami, E. Berman, Y. Cohen, Diffusion- and T2-weighted MRI of closed-head injury in rats: a time course study and correlation with histology, Magn. Reson. Imaging 15 (1997) 77–85.
[5] T. Baba, M. Moriguchi, Y. Natori, C. Katsuki, T. Inoue, M. Fukui, Magnetic resonance imaging of experimental rat brain tumors: histopathological evaluation, Surg. Neurol. 34 (1990) 378–382.
[6] N. Ben Horin, S. Hazvi, P. Bendel, R. Schul, The ontogeny of a neurotoxic lesion in rat brain revealed by combined MRI and histology, Brain Res. 718 (1996) 97–104.
[7] H. Benveniste, G.P. Cofer, C.A. Piantadosi, J.N. Davis, G.A. Johnson, Quantitative proton magnetic resonance imaging in focal cerebral ischemia in rat brain, Stroke 22 (1991) 259–268.
[8] M. Bobinski, M.J. de Leon, J. Wegiel, S. Desanti, A. Convit, L.A. Saint Louis, H. Rusinek, H.M. Wisniewski, The histological validation of post mortem magnetic resonance imaging-determined hippocampal volume in Alzheimer's disease, Neuroscience 95 (2000) 721–725.
[9] V. Bouilleret, A. Nehlig, C. Marescaux, I.J. Namer, Magnetic resonance imaging follow-up of progressive hippocampal changes in

a mouse model of mesial temporal lobe epilepsy, Epilepsia 41 (2000) 642–650.
[10] B.H. Braffman, R.A. Zimmerman, J.Q. Trojanowski, N.K. Gonatas, W.F. Hickey, W.W. Schlaepfer, Brain MR: pathologic correlation with gross and histopathology. 2. Hyperintense white-matter foci in the elderly, Am. J. Roentgenol. 151 (1988) 559–566.
[11] P.F. Buckley, Structural brain imaging in schizophrenia, Psychiatr. Clin. North Am. 21 (1998) 77–92.
[12] P.S. Buckmaster, F.E. Dudek, Neuron loss, granule cell axon reorganization, and functional changes in the dentate gyrus of epileptic kainate-treated rats, J. Comp. Neurol. 385 (1997) 385–404.
[13] K. Bulloch, M. Sadamatsu, A. Patel, B.S. McEwen, Calcitonin gene-related peptide immunoreactivity in the hippocampus and its relationship to cellular changes following exposure to trimethyltin, J. Neurosci. Res. 55 (1999) 441–457.
[14] H.M. Carelton, in: Carelton's Histological Technique, 5th Edition, Oxford University Press, New York, 1985.
[15] A. Convit, M.J. de Leon, C. Tarshish, S. De Santi, W. Tsui, H. Rusinek, A. George, Specific hippocampal volume reductions in individuals at risk for Alzheimer's disease, Neurobiol. Aging 18 (1997) 131–138.
[16] J.C. de la Torre, K. Butler, P. Kozlowski, T. Fortin, J.K. Saunders, Correlates between nuclear magnetic resonance spectroscopy, diffusion weighted imaging, and CA1 morphometry following chronic brain ischemia, J. Neurosci. Res. 41 (1995) 238–245.
[17] M.J. de Leon, A. Convit, A.E. George, J. Golomb, S. De Santi, C. Tarshish, H. Rusinek, M. Bobinski, C. Ince, D. Miller, H. Wisniewski, In vivo structural studies of the hippocampus in normal aging and in incipient Alzheimer's disease, Ann. NY Acad. Sci. 777 (1996) 1–13.
[18] R.J. Fiel, J.J. Alletto, C.M. Severin, P.A. Nickerson, M.A. Acara, R.J. Pentney, MR imaging of normal rat brain at 0.35 T and correlated histology, J. Magn. Reson. Imaging 1 (1991) 651–656.
[19] G.A. Johnson, M.B. Thompson, B.P. Drayer, Three-dimensional MRI microscopy of the normal rat brain, Magn. Reson. Med. 4 (1987) 351–365.
[20] H. Kim, G. Bing, W. Jhoo, K.H. Ko, W.K. Kim, J.H. Suh, S.J. Kim, K. Kato, J.S. Hong, Changes of hippocampal Cu/Zn-superoxide dismutase after kainate treatment in the rat, Brain Res. 853 (2000) 215–226.
[21] M.D. King, N. van Bruggen, R.G. Ahier, J.E. Cremer, J.V. Hajnal, S.R. Williams, M. Doran, Diffusion-weighted imaging of kainic acid lesions in the rat brain, Magn. Reson. Med. 20 (1991) 158–164.
[22] S.M. Lawrie, S.S. Abukmeil, Brain abnormality in schizophrenia. A systematic and quantitative review of volumetric magnetic resonance imaging studies, Br. J. Psychiatry 172 (1998) 110–120.
[23] E.W. Lothman, R.C. Collins, Kainic acid induced limbic seizures: metabolic, behavioral, electroencephalographic and neuropathological correlates, Brain Res. 218 (1981) 299–318.
[24] S.J. Lupien, M. deLeon, S. DeSanti, A. Convit, C. Tarshish, N.P. Nair, M. Thakur, B.S. McEwen, R.L. Hauger, M.J. Meaney, Cortisol levels during human aging predict hippocampal atrophy and memory deficits, Nat. Neurosci. 1 (1998) 69–73.
[25] A.M. Magarinos, B.S. McEwen, Stress-induced atrophy of apical dendrites of hippocampal CA3c neurons: comparison of stressors, Neuroscience 69 (1995) 83–88.
[26] D.H. Mathalon, E.V. Sullivan, J.M. Rawles, A. Pfefferbaum, Correction for head size in brain-imaging measurements, Psychiatry Res. 50 (1993) 121–139.
[27] K. Minematsu, L. Li, M. Fisher, C.H. Sotak, M.A. Davis, M.S. Fiandaca, Diffusion-weighted magnetic resonance imaging: rapid and quantitative detection of focal brain ischemia, Neurology 42 (1992) 235–240.
[28] J.P. Munasinghe, G.A. Gresham, T.A. Carpenter, L.D. Hall, Magnetic resonance imaging of the normal mouse brain: comparison with histologic sections, Lab. Anim. Sci. 45 (1995) 674–679.
[29] Y. Nakasu, S. Nakasu, S. Morikawa, S. Uemura, T. Inubushi, J. Handa, Diffusion-weighted MR in experimental sustained seizures elicited with kainic acid, Am. J. Neuroradiol. 16 (1995) 1185–1192.
[30] NIH, Guide for the Care and Use of Laboratory Animals, 1985.
[31] A.B. Norman, K.J. Bertram, S.R. Thomas, R.G. Pratt, R.C. Samaratunga, P.R. Sanberg, Magnetic resonance imaging of rat brain following in vivo disruption of the cerebral vasculature, Brain Res. Bull. 26 (1991) 593–597.
[32] F. Ohl, T. Michaelis, H. Fujimori, J. Frahm, S. Rensing, E. Fuchs, Volumetric MRI measurements of the tree shrew hippocampus, J. Neurosci. Methods 88 (1999) 189–193.
[33] G. Paxinos, C. Watson, in: The Rat Brain in Stereotaxic Coordinates, 2nd Edition, Academic Press, San Diego, CA, 1986.
[34] P.R. Rapp, M. Gallagher, Preserved neuron number in the hippocampus of aged rats with spatial learning deficits, Proc. Natl. Acad. Sci. USA 93 (1996) 9926–9930.
[35] A. Righini, C. Pierpaoli, J.R. Alger, G. Di Chiro, Brain parenchyma apparent diffusion coefficient alterations associated with experimental complex partial status epilepticus, Magn. Reson. Imaging 12 (1994) 865–871.
[36] A.P. Robinson, T.M. White, D.W. Mason, Macrophage heterogeneity in the rat as delineated by two monoclonal antibodies MRC OX-41 and MRC OX-42, the latter recognizing complement receptor type 3, Immunology 57 (1986) 239–247.
[37] J.K. Saunders, I.C. Smith, J.C. MacTavish, M. Rydzy, J. Peeling, E. Sutherland, H. Lesiuk, G.R. Sutherland, Forebrain ischemia studied using magnetic resonance imaging and spectroscopy, NMR Biomed. 2 (1989) 312–316.
[38] L.C. Schmued, C. Albertson, W. Slikker Jr., Fluoro-Jade: a novel fluorochrome for the sensitive and reliable histochemical localization of neuronal degeneration, Brain Res. 751 (1997) 37–46.
[39] P.E. Shrout, J.L. Fleiss, Intraclass correlations: uses in assessing rater reliability, Psychol. Bull. 86 (1979) 420–428.
[40] G. Sperk, H. Lassmann, H. Baran, F. Seitelberger, O. Hornykiewicz, Kainic acid-induced seizures: dose-relationship of behavioural, neurochemical and histopathological changes, Brain Res. 338 (1985) 289–295.
[41] M. Takahashi, B. Fritz-Zieroth, T. Chikugo, H. Ogawa, Differentiation of chronic lesions after stroke in stroke-prone spontaneously hypertensive rats using diffusion weighted MRI, Magn. Reson. Med. 30 (1993) 485–488.
[42] S. Tanaka, T. Tanaka, S. Kondo, T. Hori, H. Fukuda, Y. Yonemasu, M. Tanaka, K. Shindo, Magnetic resonance imaging in kainic acid-induced limbic seizure status in cats, Neurol. Med. Chir. 33 (1993) 285–289.
[43] N. van Bruggen, B.M. Cullen, M.D. King, M. Doran, S.R. Williams, D.G. Gadian, J.E. Cremer, T2- and diffusion-weighted magnetic resonance imaging of a focal ischemic lesion in rat brain, Stroke 23 (1992) 576–582.
[44] Y. Wang, A. Majors, I. Najm, M. Xue, Y. Comair, M. Modic, T.C. Ng, Postictal alteration of sodium content and apparent diffusion coefficient in epileptic rat brain induced by kainic acid, Epilepsia 37 (1996) 1000–1006.
[45] C. Watson, C.R. Jack Jr., F. Cendes, Volumetric magnetic resonance imaging. Clinical applications and contributions to the understanding of temporal lobe epilepsy, Arch. Neurol. 54 (1997) 1521–1531.
[46] C.S. Woolley, E. Gould, B.S. McEwen, Exposure to excess glucocorticoids alters dendritic morphology of adult hippocampal pyramidal neurons, Brain Res. 531 (1990) 225–231.